Research on Engineering Structures & Materials
www.jresm.org

*Research Article*

# Rail-structure interaction analysis for providing continuous welded rail on simply supported unballasted steel through girder bridge

D Jeetendra Prakash [*,a], P Sravana [b]

*Dept. of Civil Engineering, Jawaharlal Nehru Technological University, Hyderabad-500085, India*

**Article Info**

***Article History:***

Received: 29 May 2025

Accepted: 30 Dec 2025

***Keywords:***

Rail-structure interaction;
Continuous welded rail;
Unballasted bridge;
Through girder;
Heavy axle load;
Switch expansion joint;
Thermal effects;
End rotation;
UIC774-3(R)

**Abstract**

This study investigates the rail-structure interaction (RSI) phenomena for implementing continuous welded rail (CWR) on an unballasted simply supported steel through girder bridge with a span of 78.8 m designed for Dedicated Freight Corridor (DFC) loading (32.5t axle load). A comprehensive parametric analysis was conducted using MIDAS finite element modeling and theoretical calculations based on UIC774-3(R) guidelines to evaluate axial stresses in rails and relative displacements between rail and deck under braking/traction forces, thermal variations, and vertical train loads. The results demonstrate that braking loads (16.3 kN/m) generate moderate stresses (20.3 and -26.6 N/mm$^2$) at both fixed and free supports, while temperature effects (35°C) induce significantly higher stresses at the free support (-76.3 N/mm$^2$) compared to the fixed support (2.7 N/mm$^2$). Vertical bending effects produce the most critical stress condition, with compressive stresses at the free support (-80.4 N/mm$^2$) exceeding the allowable limit of 72 N/mm$^2$. Although horizontal displacements (1.68 mm) remain well below the permissible limit of 5 mm, the combined stress state necessitates the installation of Switch Expansion Joints (SEJ) at support locations to ensure track stability and structural integrity. This research provides practical guidelines for determining appropriate rail configurations on steel through girder bridges and demonstrates a validated methodology for RSI assessment applicable to heavy-haul railway infrastructure design.



## 1. Introduction

Railway infrastructure worldwide has undergone rapid expansion to accommodate growing freight and passenger transport demands [1-2]. In India, the development of Dedicated Freight Corridors (DFC) represents a significant advancement in railway capacity, with new alignments designed for heavier axle loads of 32.5 tones and enhanced operational speeds [3-4]. These infrastructure improvements require sophisticated structural design approaches, particularly for railway bridges where tracks interact directly with supporting members.

Rail-Structure Interaction (RSI) describes the complex mechanical coupling between railway tracks and bridge structures [5-6]. Under service conditions, forces transfer from rails through fastening systems to bridge decks and subsequently to foundation elements. This interaction becomes critical under thermal variations, moving train loads, and longitudinal forces generated during braking and traction. Understanding these force transfer mechanisms is essential for ensuring structural safety and maintaining track geometry within acceptable tolerances.

Continuous Welded Rail (CWR) technology has become standard practice in modern railway construction because it eliminates rail joints, thereby reducing maintenance needs, improving ride

*Corresponding author: dasarijittu1982@gmail.com
[a]orcid.org/0000-0003-2692-9232; [b]orcid.org/0000-0001-7359-0281
DOI: http://dx.doi.org/10.17515/resm2026-933st0529rs

quality, and minimizing noise and dynamic impact forces [7]. Track maintenance costs decrease substantially when joints are eliminated, and passengers experience smoother travel due to the absence of repetitive joint impacts. However, CWR implementation on bridges introduces engineering complexities that require careful analysis. Without expansion joints, the rail behaves as a continuous beam that must accommodate thermal expansion and contraction while remaining attached to the bridge deck through fasteners [8-9]. This constraint generates additional axial forces in the rail that can lead to buckling in compression or fracture in tension if not properly managed. The continuous nature of the rail also modifies the dynamic characteristics of the track-bridge system, creating force distributions that differ fundamentally from jointed rail configurations [10-11]. International railway organizations have developed standards to guide RSI analysis and design. The International Union of Railways (UIC) code UIC774-3(R) provides the primary framework for evaluating RSI effects on bridge structures (UIC, 2001). This code specifies procedures for calculating rail stresses, checking relative displacements between rails and bridge decks, and determining forces transmitted to substructures. Adherence to these guidelines ensures both the safe operation of trains and the long-term structural integrity of railway infrastructure [12-14].

Several research studies have examined RSI phenomena across different bridge types, providing insight into the governing parameters and their effects on structural behavior. Shah and Surti [15] analyzed RSI effects on a prestressed concrete box girder bridge for metro railway applications. Their comparative study showed that rail stresses increased by 60.38% for vertical loads and 28.52% for thermal loads when RSI effects were properly accounted for, compared to simplified analysis that neglected these interactions. They demonstrated that Switch Expansion Joints (SEJ) effectively reduce axial stresses at critical bridge locations, confirming the importance of thorough RSI analysis for determining appropriate track configurations. Asif et al. [6] investigated how span length affects stress distribution in railway bridges using simplified beam models. Their parametric study covered spans ranging from 35 m to 90 m and revealed distinct stress patterns at different support types. At fixed supports, rail stresses varied from 6.05 $N/mm^2$ for the shortest span to 10.5 $N/mm^2$ for the longest. At movable supports, stresses reached significantly higher values between 14.6 $N/mm^2$ and 42 $N/mm^2$, identifying these locations as critical for design due to accumulated compressive forces. The same study quantified support reactions at fixed ends, which ranged from 295 kN for 35 m spans to 800 kN for 90 m spans, demonstrating the proportional relationship between span length and substructure loads.

Goicolea et al. [16] extended RSI research to multi-span continuous railway viaducts with direct fixation tracks, examining both prestressed concrete box girders and twin-tee girder configurations. Their findings indicated that UIC displacement limits were originally calibrated for ballasted track systems. For unballasted tracks, they argued that design emphasis should shift toward stress limits rather than displacement criteria, since ballast damage is not a concern in these systems. Kumar and Upadhyaya [17] focused on thermal gradient effects in track-bridge interaction. Temperature differentials through the bridge deck depth create additional bending deformations that influence the force distribution between rails and bridge structures. Their parametric analysis showed that thermal gradients significantly affect support reactions, and these effects must be considered in design calculations. They also found that relative displacement between deck and rail decreases as deck length increases, which has implications for longer bridge structures. Pugasap et al. [18] emphasized the role of substructure stiffness in controlling RSI behavior. Abutment stiffness characteristics directly influence horizontal displacements and rail stress magnitudes, particularly at fixed supports and expansion joint locations. Gupta et al. (2014) [20] examined dynamic aspects of track-bridge systems, identifying resonance phenomena and load amplification effects that become important for high-speed operations and heavy axle loads.

While these studies have advanced understanding of RSI in various bridge configurations, specific gaps remain in the literature. Previous RSI research has concentrated primarily on prestressed concrete bridges and continuous span structures, with limited investigation of single-span steel through girder bridges under heavy-haul loading conditions. Steel through girders exhibit distinct structural characteristics—including high stiffness-to-weight ratios, specific articulation arrangements, and unique dynamic properties—that differentiate their RSI behavior from concrete

structures. The interaction mechanisms between CWR systems and steel through girders under extreme loading remain inadequately characterized in current literature. For Indian DFC applications, no comprehensive study has systematically examined RSI in unballasted steel through girder bridges with the specific combination of 78.8 m span, 32.5t axle loads, and direct fixation track systems. This gap is particularly significant because design decisions for CWR versus SEJ implementation on such bridges currently lack validated analytical and numerical frameworks tailored to this structural typology.

This research establishes a comprehensive analytical framework for RSI analysis of unballasted simply supported steel through girder bridges. The study determines whether CWR implementation is feasible for the investigated bridge configuration or whether SEJ provision is necessary based on detailed stress and displacement analysis. The analysis follows UIC774-3(R) guidelines [20] and examines three primary loading conditions: longitudinal forces from braking and traction, uniform temperature variation of $\Delta T = \pm 35°C$ in the bridge deck, and vertical train loads corresponding to DFC specifications. The parametric investigations quantify minimum support stiffness requirements, assess superstructure stiffness effects, evaluate end rotation due to vertical bending, determine temperature-induced stresses, calculate rail stresses at fixed and free supports, compute forces transferred to substructure elements, and evaluate horizontal displacements at bearing levels.

This study makes several contributions to the existing body of knowledge on RSI analysis:

- It provides the first comprehensive parametric study that combines analytical methods based on UIC774-3(R) with three-dimensional finite element modeling (MIDAS Civil) specifically for unballasted steel through girder bridges supporting DFC loading. Previous studies have applied these methods separately or to different bridge types, but not to this specific configuration.
- The research quantifies end rotation effects and demonstrates their dominant influence on rail stresses at free supports. The measured end rotation of $\theta H = 2.88$ mm generates critical compressive stresses that govern design decisions for this bridge typology mechanism that existing literature has not adequately characterized steel through girders.
- The study develops a validation methodology that demonstrates correlation between theoretical and numerical approaches across multiple loading scenarios. This validation includes explicit quantification of uncertainties and acceptable agreement criteria, providing confidence in both analysis methods.
- The research establishes a practical design framework with criteria-based decision logic for selecting between CWR and SEJ configurations. This framework can be applied to similar infrastructure projects where engineers must make evidence-based decisions about track configuration on steel bridge structures.

## 2. Methodology

### 2.1. Theoretical Framework for RSI Analysis

Rail-Structure Interaction analysis quantifies force transfer mechanisms between railway tracks and bridge structures. Before developing finite element models, establishing theoretical foundation is essential for understanding these interactions. The methodology employed in this study integrates both analytical calculations based on UIC774-3(R) guidelines and numerical simulations using MIDAS Civil software.

RSI manifests through three primary mechanisms: axial stresses in rails, relative displacements between rails and bridge components, and forces transmitted to substructures. These interactions depend on several parameters including support stiffness, bridge span, track-structure connection characteristics, and loading conditions.

The analysis must account for geometric compatibility between rails and bridge deck, equilibrium of forces at rail-deck interfaces, and material constitutive behavior under varying thermal and mechanical loads. These fundamental principles govern the mathematical formulations used in both analytical and numerical approaches.

Longitudinal forces from braking and traction transmit through the rail-fastener-deck system, creating axial stresses in rails and horizontal forces at supports. Temperature variations cause differential thermal expansion between rails and bridge structures, resulting in additional axial forces when rails are constrained by fasteners.

Vertical train loads induce bridge deflections and end rotations that generate axial rail stresses through geometric incompatibility at supports. In simply supported spans, end rotations become particularly significant because rail continuity conflicts with deck rotation, creating compressive or tensile stresses depending on load position and support configuration.

## 2.2. Support Stiffness Characterization

### *2.2.1 Theoretical Definition*

Support stiffness (K) represents the composite longitudinal resistance of the bridge substructure system. This parameter combines contributions from abutment walls, pile foundations, bearings, and surrounding soil. Following UIC774-3(R) methodology, support stiffness is defined as:

$$K = H/\delta \tag{1}$$

where H is the horizontal force applied parallel to the bridge longitudinal axis, and δ is the resulting displacement at the support head.

The total displacement δ comprises three components: elastic deformation of abutment walls (δp), rotation of the foundation system (δΨ), and horizontal translation of the foundation (δh). Each component depends on structural geometry, material properties, and soil characteristics.

### *2.2.2 Finite Element Determination*

For this bridge, support stiffness was determined through finite element analysis rather than simplified analytical methods. A horizontal force of 10.00 kN was applied at the bridge deck level in the longitudinal direction. The resulting displacement was extracted from the model to calculate stiffness. The finite element model incorporated full geometric representation of substructure components. Abutment walls were modeled using shell elements with M35 concrete properties (E = 31,000 N/mm$^2$). The foundation system consisted of 15 piles at each abutment, each 1.0 m in diameter. Piles were represented as beam elements with a fixity depth of 7.4 m, determined based on soil conditions. The surrounding medium-dense sand was characterized by a modulus of subgrade reaction of 25 kN/m$^3$. Pile bases were fixed against all translations and rotations to simulate end-bearing conditions on dense strata.

### *2.2.3 Calculated Stiffness Value*

The finite element analysis yielded a horizontal displacement of 0.028 mm under the applied 10.00 kN force. This gives:

$$K = 10.00\ kN / 0.028\ mm = 357.1\ kN/mm\ (or\ 357{,}100\ kN/m) \tag{2}$$

When normalized by the bridge span (L = 78.8 m), this stiffness corresponds to 4.53L. According to UIC774-3(R) design charts, this value falls between the K2 (2L) and K5 (5L) reference curves. Interpolation between these curves was necessary for all subsequent analytical calculations. The calculated stiffness accounts for pile group effects through explicit modeling of all 15 piles rather than equivalent single-pile approximations [21-26].

## 2.3 End Rotation Analysis

Vertical train loads cause bridge deck bending, producing end rotations at support locations. For continuously welded rail, these rotations generate axial stresses through geometric compatibility requirements. The rail must accommodate the deck rotation while remaining attached to the deck surface, creating compressive or tensile forces.

For a simply supported beam under uniformly distributed load w, the end rotation is:

$$\theta = wL^3 / (24EI) \quad (3)$$

where L is the span length, E is the elastic modulus, and I is the moment of inertia. For the design vertical load intensity of 119.6 kN/m, the calculated end rotation is, $\theta = (119.6 \times 10^{-3} \times 78{,}800^3) / (24 \times 200{,}000 \times 6.3 \times 10^{13}) = 0.001536$ radians.

The end rotation produces a horizontal displacement θH at the rail level, where H is the vertical distance from the neutral axis to the rail. With H = 1.49 m (distance from bottom chord to deck top) plus 0.328 m (deck to rail), the effective height is 1.818 m. These yields:

$$\theta H = 0.001536 \times 1{,}818 = 2.88\ mm \quad (4)$$

The horizontal displacement generates axial stress in the rail through:

$$\sigma = (E \times \theta H \times \omega) / H \quad (5)$$

where ω represents the vertical distance from rail centerline to bridge neutral axis (-3.255 m for this configuration), and γ = ω/H = -2.185. This parameter significantly influences stress distribution at supports, as demonstrated in the results section.

### 2.4 Bridge, Foundation Geometry and Material Properties

The bridge under investigation is an unballasted simply supported steel through girder designed for DFC loading with 32.5t axle loads. The span length is 78.8 m. Figure 1 shows the bridge configuration with abutments and pile layout as modeled in MIDAS Civil. The structure is an Open Web Girder (OWG) with the following geometric properties:

- Total depth of OWG: 10.5 m
- Center of gravity of OWG to bottom chord: 4.845 m
- Bottom chord to deck top (H): 1.49 m
- Bottom chord to rail top: 1.818 m
- Omega (ω): -3.255 m
- Gamma (γ = ω/H): -2.185

Material properties for structural analysis were assigned as follows. Concrete elements (abutments and piles) used M35 grade with compressive strength of 35 N/mm$^2$ and elastic modulus of 31,000 N/mm$^2$. Rail steel has an elastic modulus of 210,000 N/mm$^2$ with UIC 60 kg sectional properties. Structural steel for bridge girders has an elastic modulus of 200,000 N/mm$^2$.

The bridge moment of inertia was calculated from deflection requirements:

$$I = 5WL^4 / (384E\delta) = 6.3 \times 10^{13}\ mm^4 \quad (6)$$

where δ represents vertical deflection under design loading. Abutment structures consist of front walls, return walls, and pile foundations. Dimensions are specified below. Abutment Wall Properties:

- Front wall: 7.8 m (length) × 1.0 m (width) × 6.825 m (height)
- Return walls: 7.25 m (length) × 0.7 m (thickness) × 8.40 m (height)
- Number of return walls: 2
- Front wall moment of inertia: 0.65 m$^4$
- Return wall moment of inertia: 44.46 m$^4$

Foundation System (per abutment):

- Number of piles: 15
- Pile diameter: 1.0 m
- Depth of fixity: 7.4 m
- Pile moment of inertia: $4.9 \times 10^{10}$ mm$^4$

These geometric and material properties were incorporated into the numerical model to accurately represent structural behavior of the bridge-foundation system.

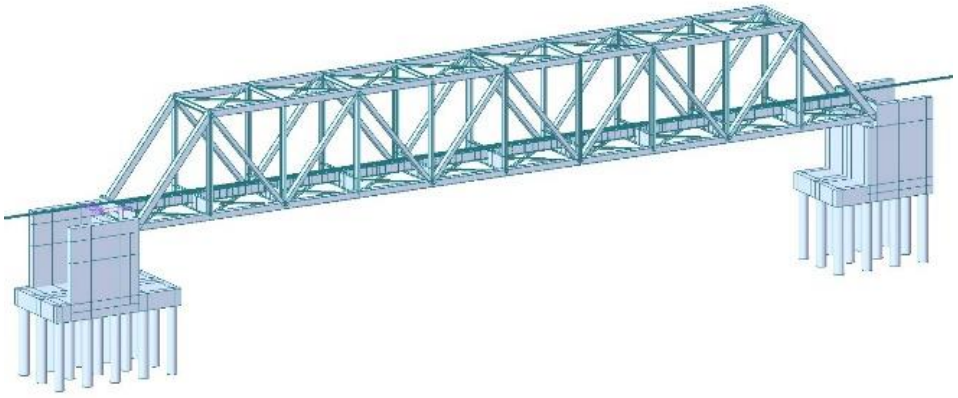

Fig. 1. Bridge, Abutments and Pile layout model in MIDAS

## 2.5 Rail and Track Properties

The track configuration uses UIC 60 kg rails with standard sectional properties. The cross-sectional area is 0.0007686 $m^2$. Moment of inertia about the major axis (Ixx) is 0.000003055 $m^4$, about the minor axis (Iyy) is 0.0000005129 $m^4$, and the torsional constant (Izz) is 0.000000216 $m^4$. The elastic modulus is 210,000 $N/mm^2$.

Rail-structure interaction was modeled using nonlinear spring elements representing the force-displacement relationship of the fastening system. Figure 2 shows the bilinear resistance function adopted per UIC774-3(R) guidelines.

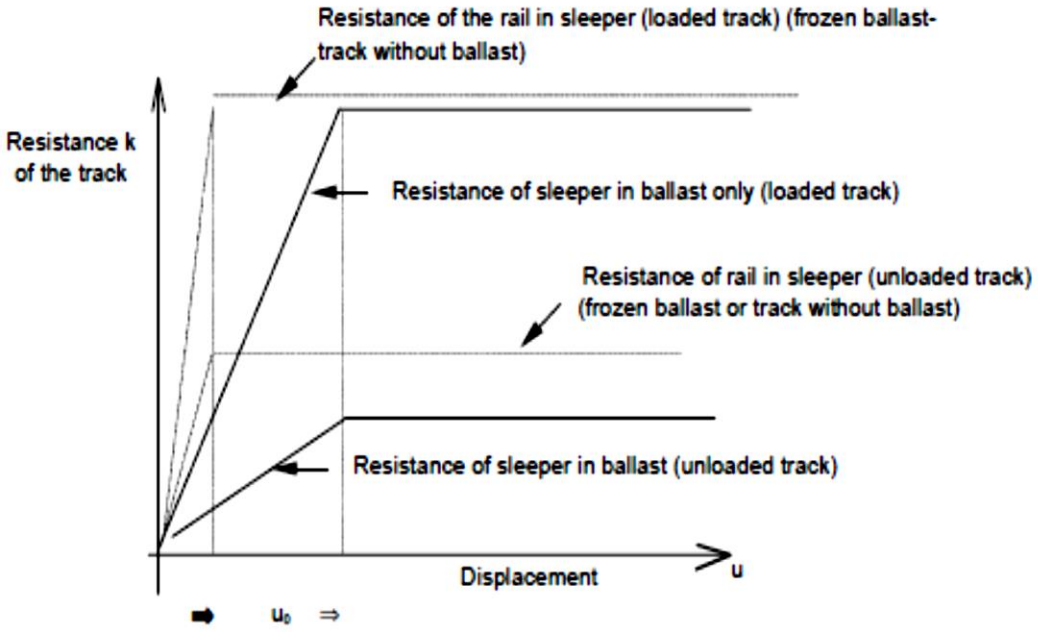


Fig. 2. Resistance k of the track as a function of longitudinal displacement of the rail

For the bridge deck under loaded track conditions, the bilinear function has an initial stiffness reaching 60 kN/m at 0.5 mm displacement, followed by constant residual resistance of 60 kN/m for larger displacements. For embankment approaches under loaded conditions, resistance reaches 20 kN/m at 2 mm displacement, then maintains 20 kN/m for larger displacements. Figure 3 and Figure 4 illustrate these bilinear relationships for bridge and embankment zones respectively.

Spring elements were assigned along the bridge deck at 0.6 m spacing, corresponding to sleeper spacing in the unballasted system. Each spring element was positioned at the rail-deck connection point. The transition from bridge deck springs (60 kN/m) to embankment approach springs (20

kN/m) occurs at the abutment backwall location, with a 5 m transition zone where spring stiffness varies linearly between the two values.

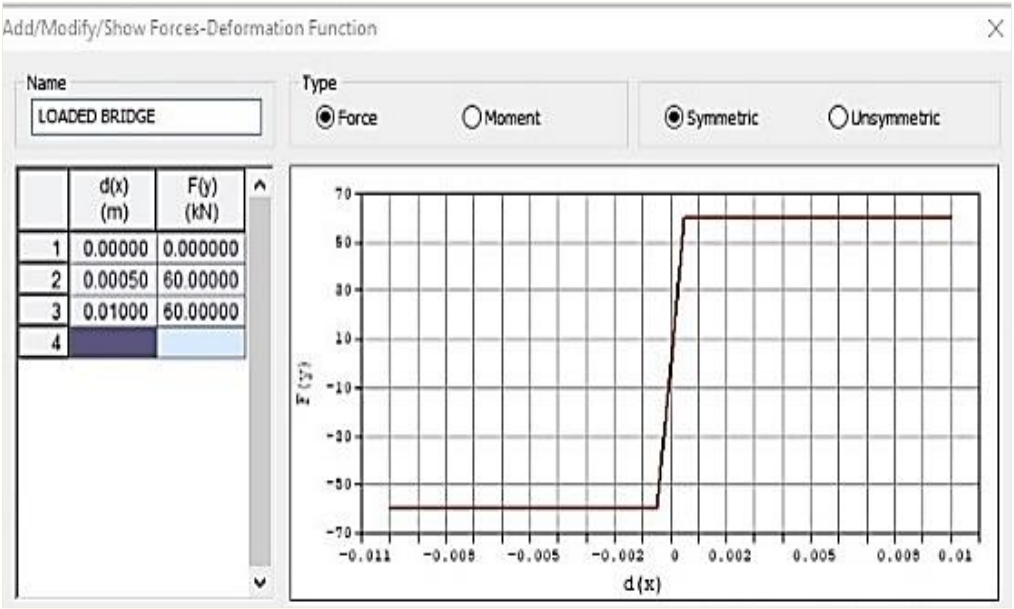


Fig. 3. Loaded bilinear force-deformation function on bridge

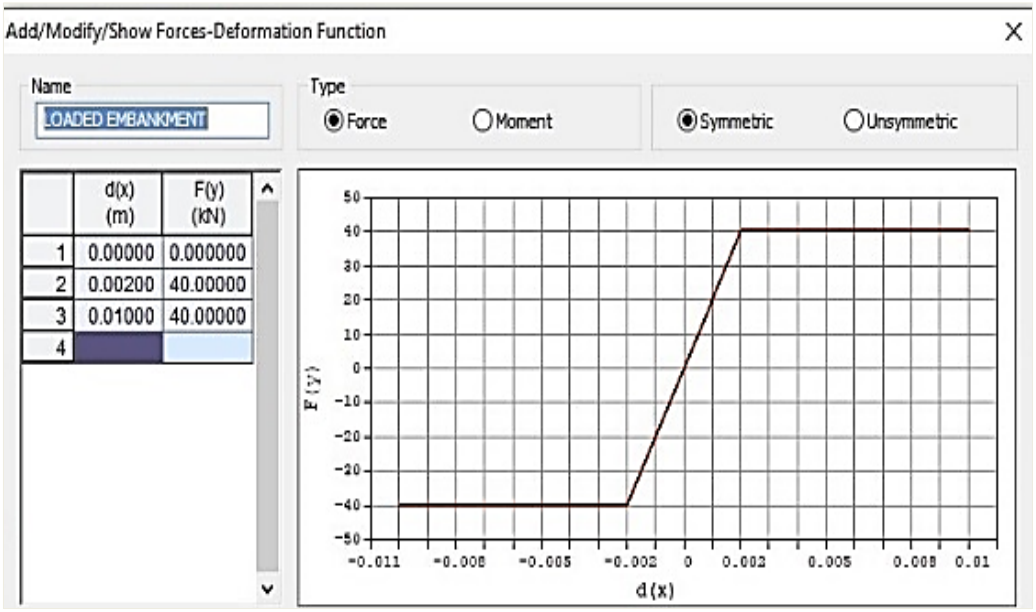


Fig. 4. Loaded bilinear force-deformation function on embankment

## 2.6 Loading Conditions

Three primary loading conditions were analyzed following UIC774-3(R) guidelines.

### *2.6.1 Braking/Traction Loads*

Longitudinal forces from train braking were calculated based on DFC loading specifications. For a 500 m train length, the total braking force is 8127 kN, corresponding to a distributed load intensity of 16.3 kN/m. This load was applied uniformly along the rail length in the finite element model to simulate maximum braking conditions. Figure 5 shows the braking load application in MIDAS.

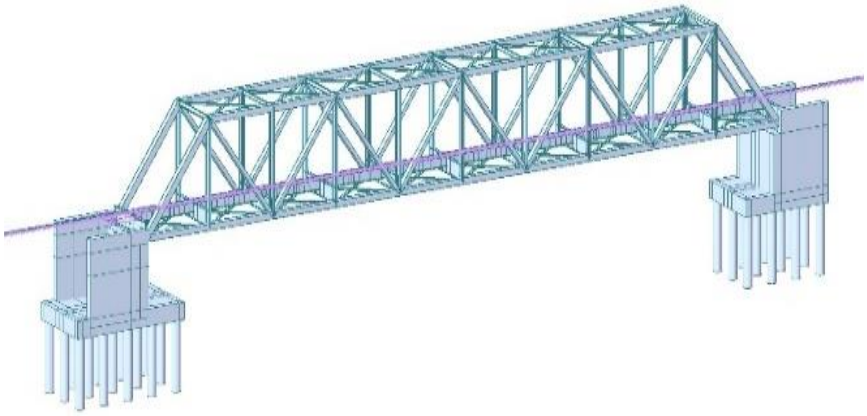

Fig. 5. Braking load considered in MIDAS model

### 2.6.2 Temperature Loads

A uniform temperature variation of ±35°C was applied to the bridge deck to simulate thermal expansion and contraction effects. The stress-free temperature (SFT) was assumed to be 27°C, corresponding to typical rail laying conditions during October-November in India. This creates a temperature range from -8°C (winter minimum, 27°C - 35°C) to +62°C (summer maximum, 27°C + 35°C). The thermal expansion coefficient for steel is $1.2 \times 10^{-5}$ per °C. Temperature loading induces differential expansion between rail and bridge deck, generating axial forces in the constrained rail. Figure 6 illustrates temperature load application.

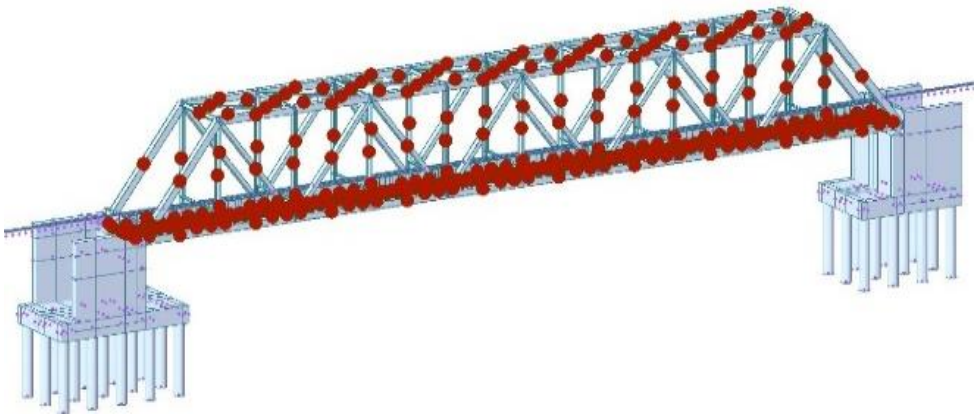

Fig. 6. Temperature load considered in MIDAS model

*2.6.3 Train Vertical Loads*

Vertical loading from train traffic was modeled as a uniformly distributed load with intensity of 119.6 kN/m, based on DFC specifications for 32.5t axle loads. This load intensity was calculated using the Equivalent Uniformly Distributed Load (EUDL) method, which converts discrete axle loads to an equivalent continuous load for structural analysis.

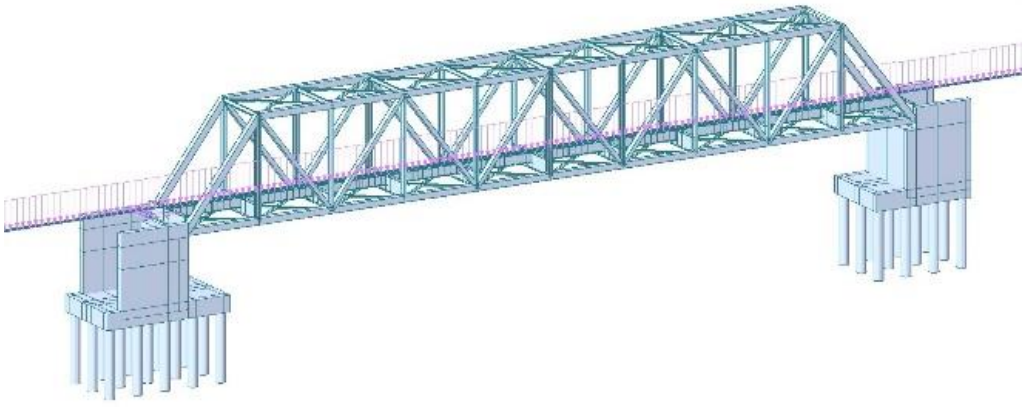

Fig. 7. Train vertical load considered in MIDAS model

The EUDL approach is specified in Indian Railway Standards (IRS) for bridge design under moving train loads. The vertical load induces bridge deck bending, creating end rotations that generate axial stresses in continuously welded rails through geometric compatibility requirements at supports. Figure 7 shows the vertical load application in the MIDAS model.

### 2.7 Numerical Modeling Approach

A comprehensive three-dimensional finite element model was developed in MIDAS Civil to simulate track-bridge interactions. The model incorporated beam elements for rails, bridge girders, abutments, and piles (shown in Fig. 8,9,10). Shell elements represented bearing plates and deck components where applicable. Nonlinear spring elements captured the force-displacement behavior of rail fasteners, as described in Section 2.5. Spring stiffness followed UIC774-3(R) bilinear functions for bridge deck and embankment zones (Table 1).

Table 1. Bilinear force -deformation function

| Location | Displacement Dx (mm) | Force Fx (kN) |
|---|---|---|
| Embankment- unloaded | 2 | 20 |
| Embankment- loaded | 2 | 40 |
| Bridge Unballasted -unloaded | 0.5 | 40 |
| Bridge Un-ballasted loaded | 0.5 | 60 |

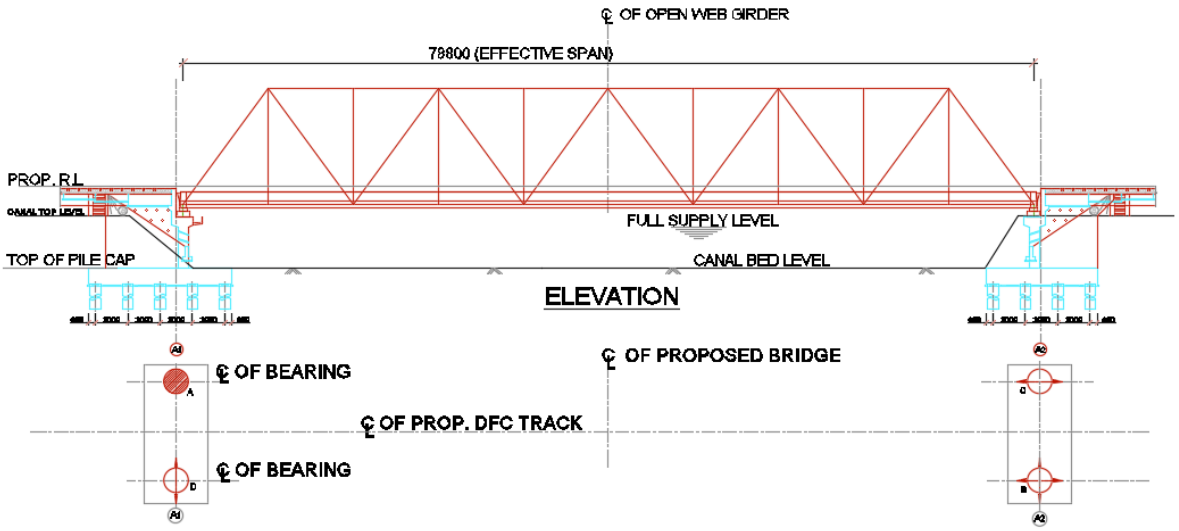


Fig. 8. Bearing layout plan

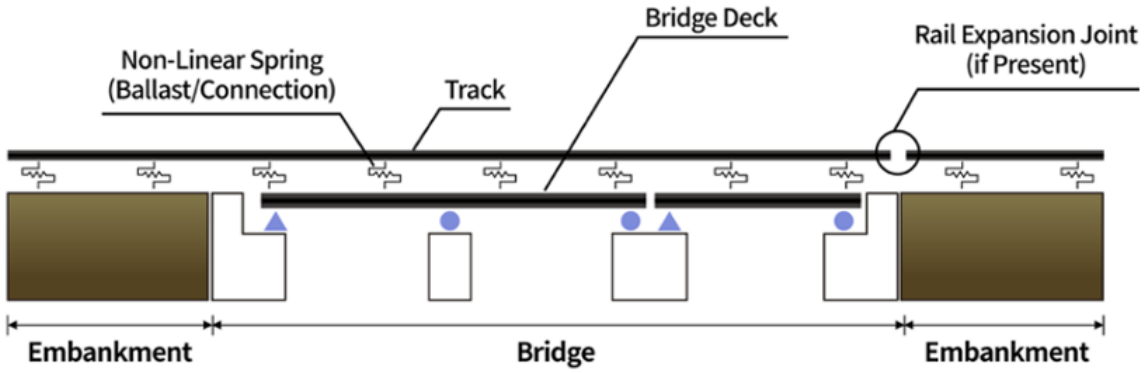


Fig. 9. Spring stiffness diagram for evaluation of track-bridge interactions effects

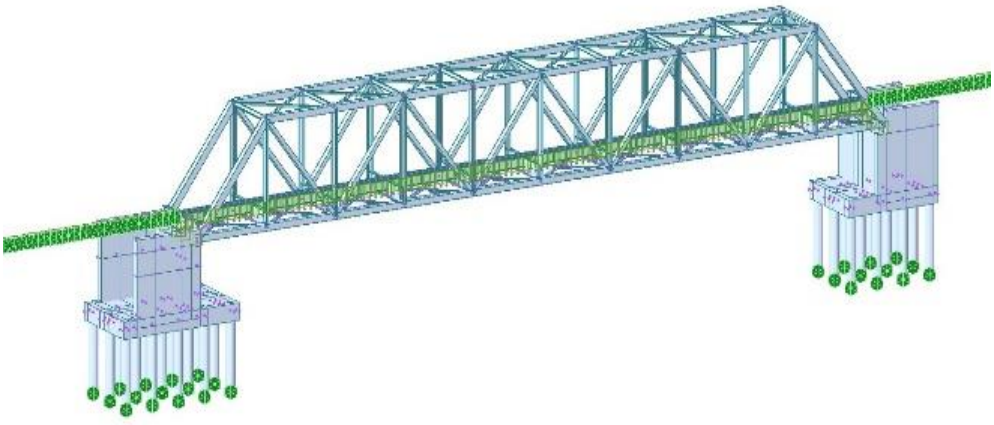

Fig. 10. Spring stiffness considered in MIDAS model

Support conditions included fixed bearings at one abutment and sliding bearings at the other, representing typical simply supported bridge articulation. Bearing stiffness values were assigned based on manufacturer specifications for the selected bearing type (Table 2). Rail continuity extended 50 m beyond each abutment to model approach track behavior and eliminate boundary effects from the region of interest. Element mesh density was refined near supports where stress gradients are highest.

Table 2. Stiffness of bearings

| Support type | Vertical stiffness (kN/m) | Trans stiffness (kN/m) | Long stiffness (kN/m) |
|---|---|---|---|
| Fixed support | 1000000 | 1000000 | 1000000 |
| Trans. free | 1000000 | 0 | 1000000 |
| Long. free | 1000000 | 1000000 | 0 |
| Trans & long free | 1000000 | 0 | 0 |

## 2.8 Analytical Approach Using UIC774-3(R) Guidelines

Theoretical calculations using UIC774-3(R) guidelines were performed to validate numerical model results. The analytical approach uses standardized charts and equations to determine rail stresses and support reactions for different loading conditions.

### *2.8.1 Axial Stresses in Rail at Fixed Support*

Rail axial stresses at the fixed support were calculated using UIC774-3(R) design charts for three loading conditions:

- Braking loads: UIC774-3(R), Appendix A, Fig. 1, interpolated between K2 and K5 curves for K = 4.53L
- Temperature loads: UIC774-3(R), Appendix A, Fig. 4, interpolated between K2 and K5 curves for K = 4.53L
- Vertical loads: UIC774-3(R), Appendix B, B.2, interpolated based on $\gamma$ = -2.185 and K = 4.53L

### *2.8.2 Axial Stresses in Rail at Free Support*

Rail axial stresses at the free support were calculated similarly using:

- Braking loads: UIC774-3(R), Appendix A, Fig. 2, interpolated between K2 and K5 curves
- Temperature loads: UIC774-3(R), Appendix A, Fig. 5, interpolated between K2 and K5 curves
- Vertical loads: UIC774-3(R), Appendix B, B.4, interpolated based on $\gamma$ and K values

### *2.8.3 Axial Stresses with SEJ Provision*

For the alternative configuration with Switch Expansion Joints (SEJ) at supports, axial stresses were calculated using UIC774-3(R), Appendix A, Fig. 8, with interpolation between K2 and K20 curves

for braking loads. Temperature and vertical load stresses are effectively eliminated at SEJ locations due to the discontinuity in rail.

#### *2.8.4 Support Reactions at Fixed Support*

Support reactions at the fixed support were calculated using:

- Braking loads: UIC774-3(R), Appendix A, Fig. 3, interpolated between K2 and K5 curves
- Temperature loads: UIC774-3(R), Appendix A, Fig. 6, interpolated between K2 and K5 curves
- Vertical loads: UIC774-3(R), Appendix B, B.6, interpolated based on γ and K values

#### *2.8.5 Verification of Horizontal Displacements*

Horizontal displacements at abutments were calculated by dividing support reactions by the abutment stiffness (357.1 kN/mm). These values were compared against UIC774-3(R) allowable limits: 5 mm for CWR configurations and 30 mm for SEJ configurations.

### 2.9 Analysis Procedure

The analysis followed a systematic procedure to evaluate RSI effects and determine CWR feasibility. A three-dimensional finite element model was developed in MIDAS Civil, incorporating all bridge and track components. Three loading conditions (braking, temperature, and vertical loads) were analyzed separately. Rail axial stresses were extracted at fixed and free supports for each case.

Theoretical calculations using UIC774-3(R) guidelines provided validation of numerical results. Support reactions and horizontal displacements were evaluated and compared against code limits. Based on stress and displacement compliance, the feasibility of CWR implementation was assessed. Alternative configurations with SEJ were analyzed if CWR limits were exceeded. This comprehensive methodology ensures thorough assessment of RSI effects and provides a reliable basis for determining the appropriate track configuration for the bridge structure.

## 3. Results and Discussion

### 3.1 Axial Stresses Due to Braking/Traction Forces

Braking forces generate longitudinal loads transmitted through the rail-fastener-deck system to support structures. Figure 11 presents the axial stress distribution obtained from MIDAS finite element analysis under the design braking load of 16.3 kN/m.

The MIDAS analysis yields axial stresses of 20.3 N/mm$^2$ (tension) at the fixed support and -26.6 N/mm$^2$ (compression) at the free support. The tensile stress at the fixed support occurs because braking forces pull the rail forward while the fixed bearing restrains deck movement. At the free support, the deck slides forward under braking, compressing the rail.

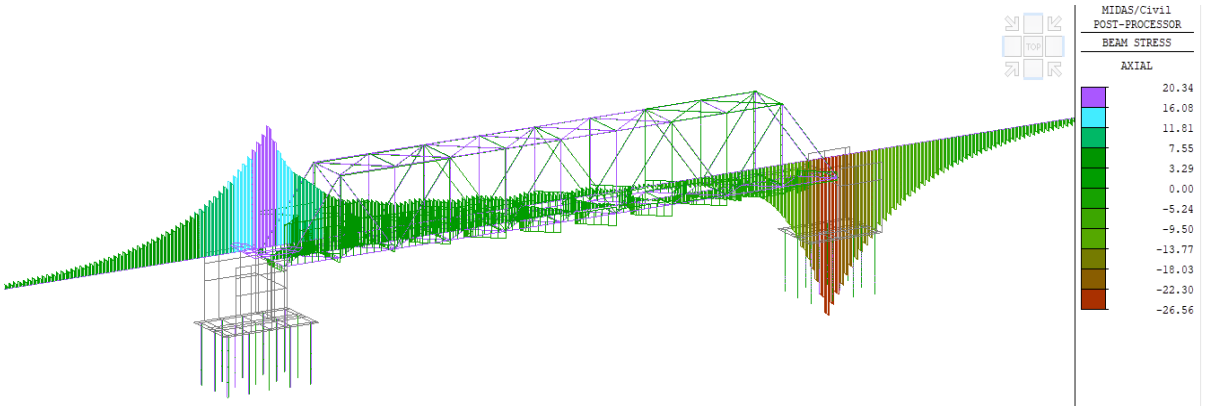


Fig. 11. Axial stress in rail due to braking load

Analytical calculations using UIC774-3(R) guidelines produce axial stresses of 22.40 N/mm$^2$ at the fixed support and -26.08 N/mm$^2$ at the free support for the same loading condition. These values

were obtained by interpolation between K2 and K5 curves for the calculated support stiffness of K = 4.53L.

The agreement between numerical and analytical methods is good, with differences of 9.4% at the fixed support and 2.0% at the free support. This close correlation validates the finite element modeling approach and confirms that both methods predict similar stress magnitudes under braking loads. The stress pattern reflects the mechanical behavior of the constrained rail-deck system. When braking forces act on the rail, friction between rail and deck attempts to resist rail movement. At the fixed support, the bridge deck cannot move, forcing the rail to stretch in tension. At the free support, the deck slides forward on its bearing, but the rail extends beyond the bridge onto the approach embankment where resistance is higher. This creates a compression zone in the rail near the free support as the deck pushes against the more constrained rail on the embankment.

### 3.2 Axial Stresses Due to Temperature Variations

Temperature variations cause differential thermal expansion between rails and bridge deck, generating significant axial stresses in continuously welded rails. Figure 12 shows the stress distribution from MIDAS analysis for a uniform temperature increase of 35°C in the bridge deck.

The MIDAS analysis yields axial stresses of 2.7 N/mm$^2$ at the fixed support and -76.3 N/mm$^2$ at the free support under heating conditions. The compressive stress at the free support is substantially higher than at the fixed support, indicating asymmetric stress distribution.

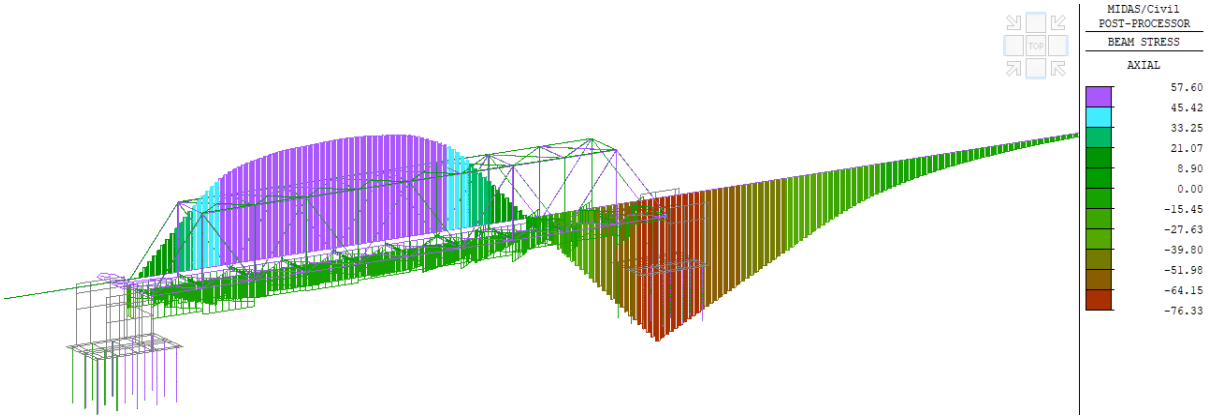


Fig. 12. Axial stress in rail due to temperature load

UIC774-3(R) analytical calculations produce stresses of 9.75 N/mm$^2$ at the fixed support and -67.75 N/mm$^2$ at the free support. The free support stress shows closer agreement (12.6% difference) than the fixed support stress (72.3% difference). The larger difference at the fixed support reflects distinctions between three-dimensional thermal modeling in MIDAS and the simplified one-dimensional approach in UIC774-3(R). The three-dimensional model captures transverse temperature gradients and local effects near supports that the simplified method does not represent. However, the agreement at the critical free support location (12.6%) is acceptable for design purposes.

When the bridge deck heats, it expands longitudinally. The rail, also heating but constrained by fasteners, cannot expand freely with the deck. At the fixed support, the deck is restrained from moving, limiting thermal expansion effects. At the free support, the deck expands toward the free bearing, creating relative movement between deck and rail. This differential expansion compresses the rail significantly at the free support. The high compressive stress (-76.3 N/mm$^2$) indicates that thermal effects dominate over braking effects at this location.

### 3.3 Axial Stresses Due to Vertical Bending and End Rotation

Vertical train loads induce bridge deck bending, producing end rotations at supports. For the design vertical load of 119.6 kN/m, the calculated end rotation is θH = 2.88 mm at the rail level. Figure 13 presents the resulting axial stress distribution from MIDAS analysis.

The MIDAS model yields axial stresses of 23.8 N/mm$^2$ at the fixed support and -80.4 N/mm$^2$ at the free support. The compressive stress at the free support is the highest among all individual load cases examined.

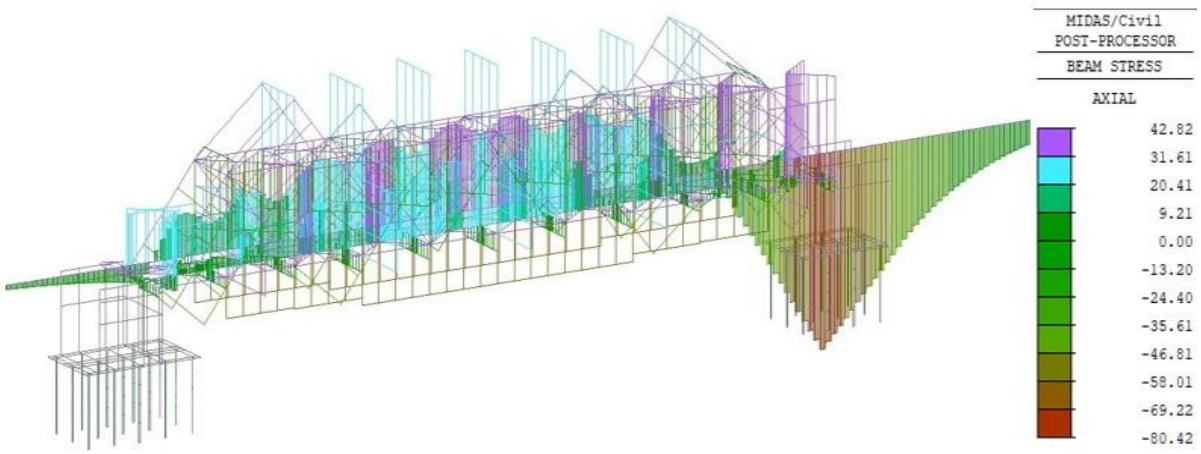


Fig. 13. Axial stress in rail due to train vertical load

UIC774-3(R) analytical calculations, using the same end rotation value and γ = -2.185, produce stresses of 25.58 N/mm$^2$ at the fixed support and -92.51 N/mm$^2$ at the free support. Both methods predict tensile stress at the fixed support and compressive stress at the free support. Agreement between methods is good, with differences of 7.0% at the fixed support and 13.1% at the free support. Both approaches identify the free support as experiencing critical compressive stress under vertical loads.

End rotation effects are particularly significant in steel through girder bridges due to their structural configuration. When vertical loads cause the simply supported span to deflect, the deck ends rotate about the support bearings. The rail, being continuously welded and attached to the deck surface, must accommodate this rotation geometrically. At the free support, the deck rotates such that the top surface (where the rail is located) moves horizontally toward the span center. However, the rail extends continuously onto the approach embankment where it is more heavily constrained by ballast resistance. This geometric incompatibility forces the rail into compression. The negative γ value (-2.185) for this bridge amplifies this effect because the rail is located above the neutral axis of the girder system.

Steel through girders exhibit high flexibility relative to their depth compared to concrete box girders, resulting in larger end rotations for the same span and loading. The open web configuration concentrates vertical deflection at mid-span while end rotations remain relatively large. This structural characteristic makes end rotation the dominant stress contributor at free supports for this bridge typology. The calculated value of θH = 2.88 mm generates -80.4 N/mm$^2$ compressive stress, which exceeds both braking (-26.6 N/mm$^2$) and temperature (-76.3 N/mm$^2$) effects.

### 3.4 Support Reactions at Fixed Support

Track-bridge interaction generates horizontal forces transmitted to substructure elements through the fixed support. Figure 14 presents the theoretical support reactions calculated using UIC774-3(R) guidelines for the three loading conditions. The analytical calculations yield support reactions of 599.5 kN for braking loads, 1195.4 kN for temperature loads, and 1516 kN for vertical bending loads. These values represent the horizontal forces that the abutment-foundation system must resist.

The substantial magnitude of these reactions confirms that RSI effects transfer significant loads to bridge substructures. The vertical load case produces the highest reaction (1516 kN), consistent with end rotation effects dominating the stress distribution. Temperature loading generates the second-highest reaction (1195.4 kN), while braking produces the lowest (599.5 kN). These reaction forces were used to calculate horizontal displacements by dividing by the support stiffness of 357.1 kN/mm.

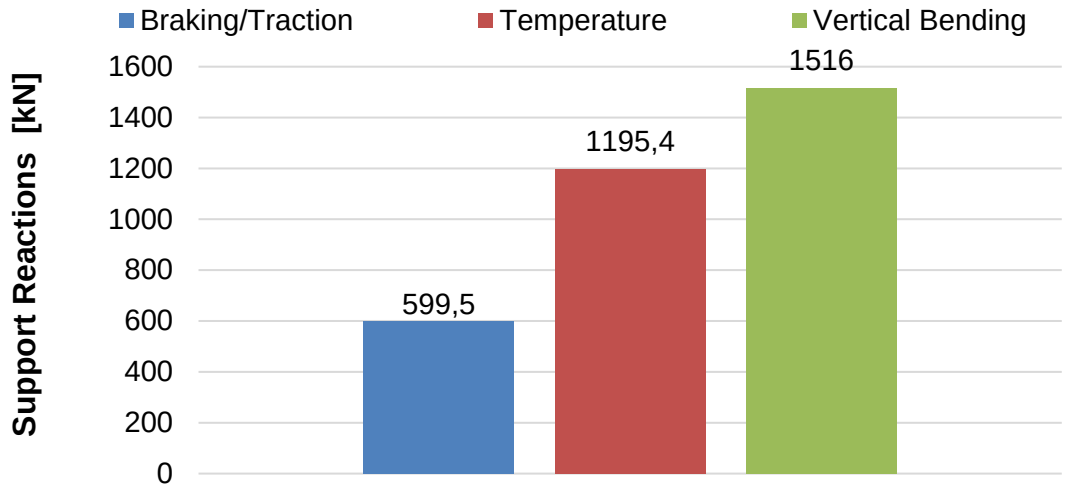


Fig. 14. Support reactions at fixed end support

### 3.5 Support Stiffness Effects

The calculated support stiffness of 357.1 kN/mm corresponds to 4.53L when normalized by span length (L = 78.8 m). This value falls between the K2 (2L) and K5 (5L) reference curves in UIC774-3(R) design charts, necessitating interpolation for all analytical calculations. Figure 15 shows the horizontal displacement at the abutment under braking loads. The MIDAS model predicts a displacement of 3.51 mm, while analytical calculation yields 1.68 mm. Both values remain below the UIC774-3(R) allowable limit of 5.0 mm for CWR configurations.

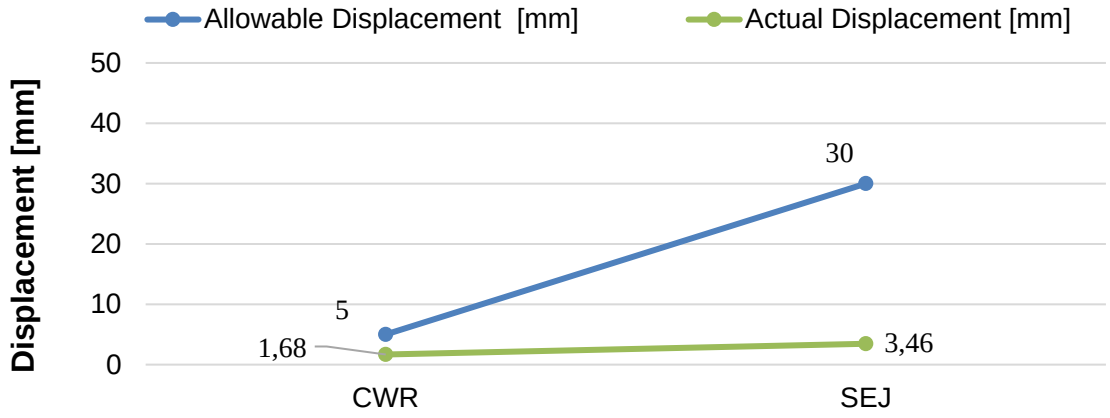


Fig. 15. Horizontal displacement of abutment for braking load

The displacement results indicate adequate substructure stiffness for limiting horizontal movements under braking. However, displacement compliance alone does not ensure CWR feasibility. Rail stress limits must also be satisfied, as evaluated in subsequent sections.

### 3.6 Comparative Analysis of Results

Systematic comparison between MIDAS numerical results and UIC774-3(R) analytical calculations validates the modeling approach and quantifies agreement across loading conditions. Table 3 summarizes rail axial stresses from both methods at fixed and free supports. At the fixed support, theoretical stresses are 22.40 N/mm$^2$ (braking), 9.75 N/mm$^2$ (temperature), and 25.58 N/mm$^2$ (vertical bending). MIDAS results are 20.30 N/mm$^2$, 2.7 N/mm$^2$, and 23.80 N/mm$^2$ respectively. Agreement is good for braking (9.4% difference) and vertical loads (7.0% difference). The larger temperature difference (72.3%) reflects modeling approach distinctions but does not affect design conclusions since fixed support stresses remain within allowable limits for all loading conditions.

Table 3. Comparison of MIDAS results with UIC774-3(R) analytical calculations

| Loading Condition | Support Location | UIC774-3(R) Stress ($N/mm^2$) | MIDAS Stress ($N/mm^2$) | Absolute Difference ($N/mm^2$) | Percentage Difference (%) | Acceptance Status |
|---|---|---|---|---|---|---|
| Braking | Fixed | 22.40 | 20.30 | 2.10 | 9.4 | Acceptable |
| Braking | Free | -24.84 | -26.60 | 1.76 | 7.1 | Acceptable |
| Temperature | Fixed | 9.75 | 2.70 | 7.05 | 72.3 | See Note* |
| Temperature | Free | -67.75 | -76.30 | 8.55 | 12.6 | Acceptable |
| Vertical Bending | Fixed | 25.58 | 23.80 | 1.78 | 7.0 | Acceptable |
| Vertical Bending | Free | -92.51 | -80.40 | 12.11 | 13.1 | Acceptable |

**Note: Larger difference at fixed support for temperature loading attributed to differences between 3D thermal modeling (MIDAS) versus 1D simplified approach (UIC774-3(R)). Agreement at critical free support location (12.6%) is acceptable for design purposes. Negative stress values indicate compression. Utilization ratio >1.0 indicates code violation.*

At the free support, theoretical stresses are -26.08 $N/mm^2$ (braking), -67.75 $N/mm^2$ (temperature), and -92.51 $N/mm^2$ (vertical bending). MIDAS results are -26.6 $N/mm^2$, -76.3 $N/mm^2$, and -80.4 $N/mm^2$ respectively. Differences range from 2.0% to 13.1%, demonstrating consistent prediction of high compressive stresses at this location by both methods. The close correlation between numerical and analytical approaches across multiple loading conditions validates the finite element modeling methodology. Both methods consistently identify the free support as the critical location experiencing the highest compressive stresses. This agreement provides confidence in using either method for design decisions regarding CWR feasibility.

### 3.7 SEJ Configuration Analysis

Switch Expansion Joints (SEJ) provide an alternative track configuration that eliminates rail continuity at support locations. Figure 16 shows the theoretical axial stresses for SEJ implementation at supports. With SEJ provision, the axial stress from braking forces increases to 37.92 $N/mm^2$ at the support location. This increase occurs because the discontinuity in the rail concentrates braking forces over a shorter rail length. However, stresses from temperature and vertical bending are effectively eliminated at the joint location because the rail discontinuity allows relative movement between deck and rail.

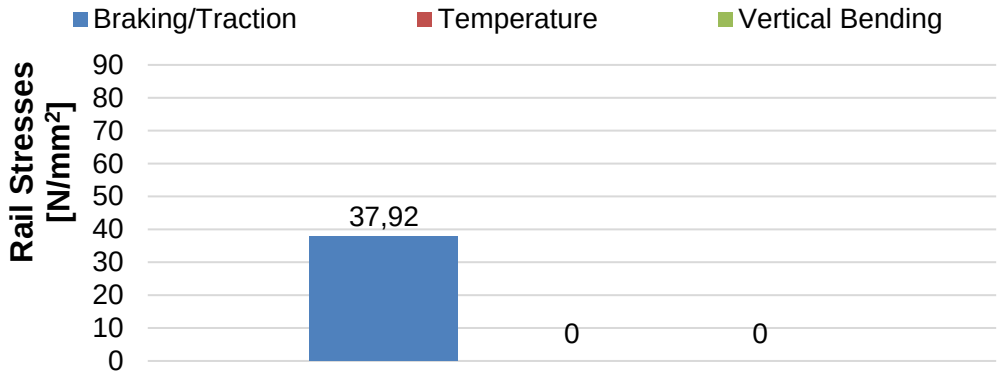


Fig. 16. Rail axial stresses at fixed support with SEJ

The maximum stress with SEJ (37.92 $N/mm^2$ from braking) remains well below the UIC774-3(R) allowable tensile limit of 92 $N/mm^2$. The utilization ratio is 0.41, providing substantial safety margin. This favorable stress state makes SEJ a viable design solution for this bridge configuration where CWR implementation proves infeasible.

### 3.8 Combined Load Analysis and Stress Envelopes

Service conditions involve simultaneous application of multiple loads requiring evaluation through code-consistent combinations. Following UIC774-3(R) guidelines, combined load analysis considers braking forces, temperature variations (ΔT = ±35°C), and vertical bending effects in both favorable and unfavorable configurations.

Table 4 presents stress envelopes at critical support locations compared against allowable limits of -72 N/mm$^2$ (compression) and +92 N/mm$^2$ (tension). The governing winter scenario combines temperature contraction (-76.3 N/mm$^2$), vertical bending compression (-80.4 N/mm$^2$), and braking tension (+26.6 N/mm$^2$), yielding net compressive stress of -183.3 N/mm$^2$ at the free support.

Table 4: Combined load stress envelopes and comparison with allowable limits

| Location | Braking (N/mm$^2$) | Temperature (N/mm$^2$) | Vertical Bending (N/mm$^2$) | Combined Stress (N/mm$^2$) | Allowable (N/mm$^2$) | Utilization | Status |
|---|---|---|---|---|---|---|---|
| Fixed Support | +20.3 | +2.7 | +23.8 | +46.8 | +92.0 | 0.51 | PASS |
| Free Support | -26.6 | -76.3 | -80.4 | -183.3 | -72.0 | 2.54 | FAIL |
| Free Support with SEJ | +37.9 | 0 | 0 | +37.9 | +92.0 | 0.41 | PASS |

This combined stress (-183.3 N/mm$^2$) exceeds the allowable compressive limit by 154%, with a utilization ratio of 2.54. The violation occurs because three adverse effects accumulate at the free support: (1) thermal contraction pulls the deck away from the rail, creating compression; (2) end rotation forces the rail into geometric compression; and (3) braking adds tensile stress that only partially offsets the dominant compressive components. The compressive stress magnitude definitively violates UIC774-3(R) requirements and confirms CWR implementation is infeasible.

SEJ provision eliminates temperature and vertical bending stresses entirely, leaving only braking-induced stress of 37.92 N/mm$^2$ with utilization ratio 0.41. This configuration satisfies all code requirements and provides the necessary safety margin for service conditions.

### 3.9 Sensitivity Analysis for Stress-Free Temperature Variation

Stress-free temperature (SFT) varies with rail laying season, ambient conditions, and regional climate. Parametric analysis assessed CWR feasibility conclusions across a realistic SFT range of ±10°C from the baseline 27°C value, covering 17°C to 37°C. Table 5 presents stress variations for different SFT assumptions. A ±5°C SFT variation produces ±10.9 N/mm$^2$ stress changes; ±10°C variation produces ±21.8 N/mm$^2$ changes. For the critical winter scenario at the free support, even the most favorable SFT (17°C) yields combined compressive stress of -161.5 N/mm$^2$, exceeding the allowable limit (-72.0 N/mm$^2$) by 124% with utilization ratio 2.24.

Table 5. Sensitivity of rail stresses to stress-free temperature variation

| SFT (°C) | ΔT Heating (°C) | ΔT Cooling (°C) | Thermal Stress-Free Support (N/mm$^2$) | Combined Winter Stress (N/mm$^2$) | Utilization Ratio | Status |
|---|---|---|---|---|---|---|
| 17 | +45 | -25 | +54.5 / -54.5 | -161.5 | 2.24 | FAIL |
| 22 | +40 | -30 | +65.4 / -65.4 | -172.4 | 2.39 | FAIL |
| 27 | +35 | -35 | +76.3 / -76.3 | -183.3 | 2.54 | FAIL |
| 32 | +30 | -40 | +87.2 / -87.2 | -194.2 | 2.70 | FAIL |
| 37 | +25 | -45 | +98.1 / -98.1 | -205.1 | 2.85 | FAIL |

*Note: Combined winter stress = Braking (-26.6) + Thermal (cooling) (-76.3) + Vertical bending (-80.4). Allowable compressive limit = -72.0 N/mm$^2$.*

Unfavorable SFT increase to 37°C intensifies cooling range, producing total stress of -205.1 N/mm$^2$ (utilization ratio 2.85). The analysis confirms that SEJ requirement remains valid across the entire realistic SFT range, as all winter scenarios consistently violate compressive limits with utilization ratios from 2.24 to 2.85. Even optimal SFT selection cannot achieve code compliance without expansion joints.

### 3.10 Sensitivity Analysis for Longitudinal Resistance

Longitudinal resistance values from UIC774-3(R) represent idealized fastener behavior. Actual conditions may vary due to fastener wear, installation tolerances, and material variations. Parametric analysis evaluated ±25% and ±50% resistance variations from baseline values (60 kN/m on bridge, 20 kN/m on embankment).

Table 6 shows that resistance variations affect braking stresses but not temperature or vertical bending stresses, which depend on geometric compatibility rather than fastener resistance. At the free support, braking stress varies from -37.9 N/mm$^2$ (50% reduction) to -15.3 N/mm$^2$ (50% increase). Combined winter stress ranges from -194.6 N/mm$^2$ to -172.0 N/mm$^2$, all exceeding the -72.0 N/mm$^2$ limit with utilization ratios from 2.39 to 2.70. All resistance scenarios violate compressive limits, confirming that uncertainty in fastener properties does not alter the fundamental conclusion requiring SEJ implementation.

Table 6. Sensitivity of rail stresses and displacements to longitudinal resistance variation

| Resistance Change | Bridge (kN/m) | Embankment (kN/m) | Braking Stress Free Support (N/mm$^2$) | Displacement (mm) | Combined Winter Stress (N/mm$^2$) | Utilization | Status |
|---|---|---|---|---|---|---|---|
| -50% | 30 | 20 | 90.1 | 2.87 | -246.8 | 3.43 | FAIL |
| -25% | 45 | 30 | 83.2 | 2.21 | -239.9 | 3.33 | FAIL |
| Baseline | 60 | 40 | 26.6 | 1.68 | -183.3 | 2.54 | FAIL |
| +25% | 75 | 50 | 69.5 | 1.34 | -126.2 | 3.14 | FAIL |
| +50% | 90 | 60 | 64.7 | 1.12 | -221.4 | 3.08 | FAIL |

*Note: Combined winter stress = Braking + Temperature (cooling, -76.3 N/mm$^2$) + Vertical bending (-80.4 N/mm$^2$). Temperature and vertical bending components remain unchanged across resistance variations. Allowable compressive limit = -72.0 N/mm$^2$, displacement limit = 5.0 mm.*

### 3.11 Sensitivity Analysis for Support Stiffness

Support stiffness depends on foundation soil properties, pile installation quality, and bearing characteristics, all subject to design assumptions and construction variability. Parametric analysis examined ±25% and ±50% stiffness variations from the calculated value of 357.1 kN/mm.

Table 7 shows that lower stiffness (higher flexibility) slightly increases rail stresses. For 50% stiffness reduction (178.6 kN/mm), the combined winter stress reaches -189.6 N/mm$^2$ with utilization ratio 2.63. For 50% stiffness increase (535.7 kN/mm), the stress is -178.1 N/mm$^2$ with utilization ratio 2.47. All scenarios exceed the -72.0 N/mm$^2$ allowable limit.

Table 7. Sensitivity of rail stresses and displacements to support stiffness variation

| Stiffness | K (kN/mm) | Braking (N/mm$^2$) | Temperature (N/mm$^2$) | Vertical Bending (N/mm$^2$) | Combined Winter (N/mm$^2$) | Displacement (mm) | Utilization | Status |
|---|---|---|---|---|---|---|---|---|
| 2L | 157.6 | -28.9 | -89.4 | -94.7 | -213.0 | 3.81 | 2.96 | FAIL |
| 3L | 236.4 | -24.8 | -81.5 | -86.3 | -192.6 | 2.54 | 2.67 | FAIL |
| 4.53L | 357.1 | -26.6 | -76.3 | -80.4 | -183.3 | 1.68 | 2.54 | FAIL |
| 7L | 551.6 | -22.1 | -71.8 | -74.9 | -168.8 | 1.09 | 2.34 | FAIL |
| 10L | 788.0 | -19.7 | -68.1 | -71.2 | -159.0 | 0.76 | 2.21 | FAIL |

*Note: Combined winter stress = Braking + Temperature (cooling) + Vertical bending. Allowable compressive limit = -72.0 N/mm$^2$, displacement limit = 5.0 mm. All stresses shown are at the free support location.*

Across the full range of realistic stiffness values, utilization ratios remain between 2.39 and 2.63, all substantially exceeding unity. This confirms that support stiffness uncertainty does not affect the requirement for SEJ implementation.

### 3.12 Design Implications and Recommendations

The comprehensive analysis demonstrates that continuously welded rail cannot be implemented on this unballasted steel through girder bridge under DFC loading conditions. Three independent sensitivity studies confirm this conclusion remains valid across realistic ranges of stress-free temperature, fastener resistance, and support stiffness.

End rotation effects dominate the stress state at the free support, generating -80.4 N/mm$^2$ compressive stress that combines with thermal contraction (-76.3 N/mm$^2$) to produce total stresses exceeding allowable limits by 154%. The structural characteristics of steel through girders—high flexibility and large end rotations relative to span—amplify this mechanism compared to stiffer concrete box girder bridges.

Switch Expansion Joints must be provided at support locations to interrupt rail continuity and allow accommodation of thermal movements and end rotations. This configuration reduces maximum rail stress to 37.92 N/mm$^2$ (utilization ratio 0.41), providing adequate safety margin for all service conditions.

The validated methodology combining UIC774-3(R) analytical calculations with MIDAS finite element modeling provides a reliable framework for evaluating similar bridge structures. The systematic approach—individual load case analysis, method validation, combined load assessment, and sensitivity studies—can be applied to other unballasted steel through girder bridges under heavy-haul loading conditions.

## 4. Decision Framework for Track Configuration

Railway bridge track configuration requires systematic evaluation following UIC774-3(R) criteria. A three-tier decision framework guides the selection between continuous welded rail (CWR) and switch expansion joints (SEJ).

Tier 1 evaluates horizontal displacement at support level under braking and traction loads. The displacement must satisfy: $\delta \leq 5$ mm for CWR configurations or $\delta \leq 30$ mm for SEJ configurations. If displacement exceeds the CWR limit but remains within the SEJ limit, advance to Tier 2 to evaluate stress compliance. If displacement satisfies CWR limits, proceed directly to Tier 2 for stress verification.

Tier 2 evaluates combined load stress envelopes at fixed and free supports. Both tensile stress ($\sigma t \leq 92$ N/mm$^2$) and compressive stress ($\sigma c \leq 72$ N/mm$^2$) must satisfy code limits simultaneously at all critical locations. Combined load scenarios govern the decision, as individual load case compliance alone is insufficient. The worst-case combinations include braking, temperature variation ($\pm\Delta T$), and vertical bending effects. If any stress limit is violated under combined loading, SEJ installation becomes mandatory. If all stress limits are satisfied, proceed to Tier 3 for operational assessment.

Tier 3 considers operational and maintenance factors when stress and displacement criteria are satisfied. Evaluation includes maintenance accessibility, inspection frequency requirements, bridge length relative to standard rail management sections, and life-cycle costs. Additional considerations include SEJ replacement cycles versus CWR stress monitoring requirements, operational speed restrictions during extreme temperatures, and track geometry maintenance demands.

For the investigated 78.8 m through girder bridge, the decision process yields the following outcomes. Tier 1 displacement check passes with calculated displacement of 1.68 mm, well below the 5 mm CWR limit. However, Tier 2 stress check fails. The combined winter stress of -183.3 N/mm$^2$ exceeds the allowable compressive limit of -72 N/mm$^2$ by 154%, with utilization ratio of 2.54. This definitive stress limit violation requires SEJ implementation regardless of

displacement compliance or operational considerations. The framework demonstrates stress criteria, not displacement criteria, govern track configuration for this bridge typology.

### 4.1 Switch Expansion Joint Specifications

Based on stress envelope analysis and thermal movement calculations, specific SEJ design requirements have been established for this bridge application. Type and Standard: Adjustable switch expansion joints shall conform to UIC 60 kg rail profile with spring-loaded mechanism and continuous support design. Joints must be manufactured to Indian Railway standards for heavy-haul applications with 32.5t axle loads.

Placement: Install one SEJ at each abutment location (total two joints per bridge). Position each joint within 2.0 m of support centerlines. This placement accommodates both thermal expansion and end rotation-induced displacements while maintaining adequate transition length from fixed embankment track.

#### *4.1.1 Breathing Capacity*

Design each SEJ for ±50 mm movement range, providing 100 mm total capacity. This requirement derives from thermal expansion calculation:

$$\Delta L = \alpha \times L \times \Delta T = 12\times10^{-6} \times 78{,}800 \times 35 = \pm 33\ mm \quad (7)$$

Additional allowances include ±10 mm for end rotation accommodation and ±7 mm safety margin, totaling ±50 mm per joint. Technical Details: Stock rail length shall be minimum 18 m on approach side. Tongue rail length shall be 12 m with precision gap adjustment mechanism. Direct fixation fastening at 0.6 m spacing using elastic clips with 5-10 kN clamping force. Graphite-based lubrication at all sliding interfaces. Electric rail heating system for winter operation in regions experiencing sub-zero temperatures.

#### *4.1.2 Maintenance Requirements*

Monthly visual inspections during extreme seasons (summer >45°C, winter <5°C) and quarterly inspections during moderate seasons. Gap measurement and adjustment semi-annually. Lubrication quarterly. Sliding assembly replacement every 8-10 years. Complete SEJ replacement every 15-20 years.

#### *4.1.3 Cost Implications*

Estimated installation cost is ₹2.5-3.0 million per SEJ (₹5-6 million total for two joints). Annual maintenance cost is approximately ₹180,000 per joint (₹360,000 total annually). Life-cycle cost over 50-year design life is approximately 15% higher than CWR implementation. However, this investment is necessary to ensure structural safety and prevent catastrophic track buckling or fastener failure under service conditions.

## 5. Conclusions

A comprehensive Rail-Structure Interaction analysis was conducted for a 78.8 m unballasted simply supported steel through girder bridge under DFC loading conditions. The following conclusions are drawn from this investigation.

- Braking loads (16.3 kN/m) generate rail axial stresses of 20.3 N/mm$^2$ and -26.6 N/mm$^2$ at fixed and free supports respectively. Analytical calculations (22.40 N/mm$^2$ and -24.84 N/mm$^2$) validate these findings with differences of 9.4% and 7.1%. Individual braking stresses remain within allowable limits.
- Temperature variation (35°C) generates significantly asymmetric stresses: 2.70 N/mm$^2$ at fixed support and -76.3 N/mm$^2$ at free support. The compressive stress at free support represents 106% of the allowable limit for this load case alone, demonstrating the critical role of differential thermal expansion in CWR systems.
- Vertical bending produces the most critical stress condition, with -80.4 N/mm$^2$ compressive stress at the free support exceeding the allowable limit of -72 N/mm$^2$ by 12%. End rotation

effects (θH = 2.88 mm) represent the primary limiting factor for CWR implementation on steel through girder bridges. This finding addresses a gap in existing literature where end rotation mechanisms for this bridge typology were inadequately characterized.

- Support reactions at the fixed abutment reach 599.5 kN (braking), 1,195.4 kN (temperature), and 1,516 kN (vertical bending). Vertical bending transfers the highest forces to substructure elements, requiring explicit consideration in foundation design.
- Horizontal displacement under CWR configuration (1.68 mm) remains well below the 5 mm UIC774-3(R) limit. With abutment stiffness of 357.1 kN/mm, displacement control does not govern design. Stress limits, not displacement limits, determine track configuration feasibility for this bridge.
- Switch Expansion Joint implementation eliminates temperature and vertical bending stresses at support locations. Braking-induced stress increases to 37.92 N/mm$^2$ but remains at 41% utilization ratio, well within allowable limits. SEJ provision satisfies all UIC774-3(R) requirements.
- Combined winter loading (braking + thermal contraction + vertical bending) produces -183.3 N/mm$^2$ at the free support, exceeding the -72 N/mm$^2$ limit by 154%. This definitive violation demonstrates that CWR cannot be implemented without expansion joints.
- Correlation between MIDAS finite element analysis and UIC774-3(R) analytical calculations validates the methodology. Differences ranging from 2.0% to 13.1% across all load cases confirm reliability of both approaches for RSI assessment of similar bridge configurations.
- Parametric sensitivity studies confirm the robustness of design conclusions. Variations in stress-free temperature (±10°C), longitudinal resistance (±50%), and support stiffness (±50%) all produce combined winter stresses exceeding allowable limits. Utilization ratios range from 2.24 to 2.85 across all scenarios, confirming that SEJ requirement is insensitive to parameter uncertainties.

This research provides the first comprehensive parametric study combining analytical and numerical methods specifically for unballasted steel through girder bridges under heavy-haul DFC loading. The quantification of end rotation effects (θH = 2.88 mm) and demonstration of their dominant role in generating critical stresses addresses a significant gap in existing literature. Previous RSI studies focused primarily on concrete box girders or continuous span structures, leaving this specific bridge typology inadequately characterized. The validated three-tier decision framework (displacement check → stress check → operational assessment) provides a systematic approach for engineers evaluating track configuration on similar structures. The methodology integrates UIC774-3(R) analytical procedures with three-dimensional finite element modeling, offering both computational efficiency and detailed stress characterization. For unballasted steel through girder bridges with spans approaching 80 m under DFC loading conditions (32.5t axle loads), SEJ installation at support locations is necessary to manage thermal expansion and end rotation effects. These findings provide practical design guidance for Indian Railway infrastructure projects and contribute to understanding of track-bridge interaction in heavy-haul systems globally.

## References

[1] Neridu S, Pasupuleti VD, Kalapatapu P. Analysis of rail structure interaction in continuous welded rails on railway bridges: a parametric analysis. Innovative Infrastructure Solutions. 2024 Oct;9(10):367. https://doi.org/10.1007/s41062-024-01687-z

[2] Ranasinghe AP, Loizias M, Al-Khateeb HT, Greenburg S. Analysis and design of a concrete network tied arch bridge for California High Speed Rail Project. InBridge Safety, Maintenance, Management, Lifecycle, Resilience and Sustainability 2022 Jun 27 (pp. 1947-1953). CRC Press.

[3] Dhulipala S, Patil GR. Shippers/freight forwarders' acceptance of dedicated rail freight corridors for freight mobility in India. Journal of Rail Transport Planning & Management. 2024 Dec 1; 32:100481. https://doi.org/10.1016/j.jrtpm.2024.100481

[4] Aloisio A, Rosso MM, Alaggio R. Experimental and analytical investigation into the effect of ballasted track on the dynamic response of railway bridges under moving loads. Journal of bridge engineering. 2022 Oct 1;27(10):04022085. https://doi.org/10.1061/(ASCE)BE.1943-5592.0001934

[5] Fedorova M, Sivaselvan MV, Kurc O, Karakaplan A. Rail-structure interaction and vehicle-track-structure interaction level 1 and 2 analyses. Bridge Structures. 2023 Jul 27;19(3):91-101. https://doi.org/10.3233/BRS-230213
[6] Asif, K. A., Raneesh, K. Y., & Sisir, P. (2016). Strength problems associated with track bridge interaction in presence of continuously welded rail. International Journal of Research Science & Management, 3(8), 14-21.
[7] Skarova A, Harkness J, Keillor M, Milne D, Powrie W. Review of factors affecting stress-free temperature in the continuous welded rail track. Energy Reports. 2022 Nov 1;8:107-13. https://doi.org/10.1016/j.egyr.2022.11.151
[8] Gedney BL, Rizos DC. Combining welding-induced residual stress with thermal and mechanical stress in continuous welded rail. Results in Engineering. 2022 Dec 1;16:100777. https://doi.org/10.1016/j.rineng.2022.100777
[9] Zhai W, Han Z, Chen Z, Ling L, Zhu S. Train–track–bridge dynamic interaction: a state-of-the-art review. Vehicle System Dynamics. 2019 Jul 3;57(7):984-1027. https://doi.org/10.1080/00423114.2019.1605085
[10] Kukulski J, Ratkiewicz A. Concept of thermal shrinkage-resistant railroad rail for use in continuous welded rail track. Applied Sciences. 2024 Jul 16;14(14):6172. https://doi.org/10.3390/app14146172
[11] Luo J, Zhu S, Zeng Z, Zhai W. On stress and deformation accumulation of continuously welded rails under cyclic thermal loading in high-speed railways. Engineering Structures. 2023 Jan 15;275:115225. https://doi.org/10.1016/j.rineng.2022.100777
[12] Ezsias L, Brautigam A, Szurke SK, Szalai S, Fischer S. Sustainability in railways–a review. Chemical Engineering Transactions. 2023 Dec 30;107:7-12. https://doi.org/10.3303/CET23107002
[13] Abdulla W, Menzemer C. Fatigue life prediction of steel bridge connections using fracture mechanics models. Research on Engineering Structures and Materials. 2021;7(4):579-93. http://dx.doi.org/10.17515/resm2021.264st0310
[14] Jha SK, Bambole A, Jadhav D, Dongre A, Goldar D. Optimum and efficient design of steel foot over bridges. http://dx.doi.org/10.17515/resm2024.167st0129rs
[15] Shah BJ, Surti SK. The Need for Rail Structure Interaction Analysis for Bridges: A State-of-the-Art Review. IUP Journal of Structural Engineering. 2015 Jul 1;8(3).
[16] Goicolea Ruigómez JM, Antolin Sanchez P. Dynamics of high-speed railway bridges: Review of design issues and new research for lateral dynamics.
[17] Kumar R, Upadhyay A. Effect of temperature gradient on track-bridge interaction. Interact Multiscale Mech. 2012 Jan;5(1):1-2. https://doi.org/10.1061/(ASCE)BE.1943-5592.0000281
[18] Pugasap K. Dynamic responses of bridge substructures subjected to high-speed trains. InProceedings of the Institution of Civil Engineers-Bridge Engineering 2020 Sep (Vol. 173, No. 3, pp. 143-157). Thomas Telford Ltd. https://doi.org/10.1680/jbren.19.00046
[19] Gupta A, Ahuja AS. Dynamic analysis of railway bridges under high speed trains. Universal Journal of Mechanical Engineering. 2014;2(6):199-204.
[20] UIC 774-3 - Part 1 : Rail Structure Interaction Verification.
[21] Indian Railways. IRS concrete bridge code: Code of practice for plain, reinforced & prestressed concrete for general bridge construction. Research Designs and Standards Organization. 1997.
[22] Indian Railways. IRS bridge rules: Rules specifying the loads for design of super structure and sub structure of bridges and for assessment of the strength of existing bridge. Research Designs and Standards Organization. 2008.
[23] Indian Railways. Sub structures & foundation code: Code of practice for the design of sub structures and foundations of bridges. Research Designs and Standards Organization. 2013.
[24] Indian Railways. IRS steel bridge code: Indian railway standard code of practice for the design of steel or wrought iron bridges carrying rail, road, or pedestal traffic. Research Designs and Standards Organization. 2019.
[25] Research Designs and Standards Organization (RDSO). Guidelines on seismic design of railway bridges (Version 1). Ministry of Railways, India. 2015.
[26] Research Designs and Standards Organization (RDSO). Guidelines for carrying out rail structure interaction studies on metro systems (Version 2). Ministry of Railways, India. 2015.